

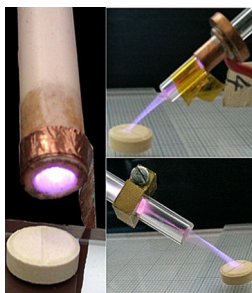
## RESEARCH ARTICLE

# Comparison of Three Plasma Sources for Ambient Desorption/Ionization Mass Spectrometry

Kirsty McKay,<sup>1</sup> Tara L. Salter,<sup>2</sup> Andrew Bowfield,<sup>1,2</sup> James L. Walsh,<sup>1</sup> Ian S. Gilmore,<sup>2</sup> James W. Bradley<sup>1</sup>

<sup>1</sup>Department of Electrical Engineering and Electronics, University of Liverpool, Brownlow Hill, L69 3GJ, UK

<sup>2</sup>Surface and Nanoanalysis Group, National Physical Laboratory, Teddington, TW11 0LW, UK



**Abstract.** Plasma-based desorption/ionization sources are an important ionization technique for ambient surface analysis mass spectrometry. In this paper, we compare and contrast three competing plasma based desorption/ionization sources: a radio-frequency (rf) plasma needle, a dielectric barrier plasma jet, and a low-temperature plasma probe. The ambient composition of the three sources and their effectiveness at analyzing a range of pharmaceuticals and polymers were assessed. Results show that the background mass spectrum of each source was dominated by air species, with the rf needle producing a richer ion spectrum consisting mainly of ionized water clusters. It was also seen that each source produced different ion fragments of the analytes under investigation:

this is thought to be due to different substrate heating, different ion transport mechanisms, and different electric field orientations. The rf needle was found to fragment the analytes least and as a result it was able to detect larger polymer ions than the other sources.

**Keywords:** Plasma sources, Ambient mass spectrometry, Desorption/ionization processes

Received: 10 February 2014/Revised: 8 April 2014/Accepted: 3 May 2014/Published online: 4 June 2014

## Introduction

The field of ambient surface analysis mass spectrometry is rapidly expanding, with applications covering many different scientific and technological areas such as pharmaceuticals [1–3], environmental science [4], and forensics [5]. Recent developments in the field have seen increased utilization of atmospheric-pressure plasmas as ambient ionization sources; techniques include low-temperature plasma (LTP) ionization [6–8], direct analysis in real-time (DART) [9, 10], flowing atmospheric-pressure afterglow (FAPA) [11], dielectric barrier discharge ionization (DBDI) [12, 13], and plasma assisted desorption/ionization (PADI) [2, 14, 15]. All plasma-based sources take advantage of the unique properties of non-equilibrium atmospheric pressure plasmas, however, the various techniques exhibit different electrical and physio/chemical properties that are influenced by factors including electrode configuration and excitation mechanism [16, 17]. As a result of these differing properties, the processes through which individual plasma sources desorb/ionize surface compounds could potentially differ significantly. To further complicate the situation, factors

such as sample temperature and angle of incidence at the surface have also been shown to affect the desorption and ionization processes [15].

In this study, we use mass spectrometry to explore the mechanisms through which three of these plasma sources desorb/ionize surface material and discuss how differences in electric field, transport mechanisms, chemistry, and temperature influence this process. The three sources considered were a rf plasma needle (PADI), a dielectric barrier plasma jet, and low-temperature plasma probe (LTP). These plasma sources have been chosen because of their widespread use in plasma physics and in surface analysis, and each source is described below.

The plasma needle source operates as an rf corona discharge, in which a high electric field is created at the tip of the sharp needle [18]. The electric field produced in this configuration is perpendicular to the direction of gas flow and, as a result, the discharge does not directly interact with the surface [19]. For the conditions considered in this paper, the rf plasma needle operates in the high power glow discharge mode, this mode is characterized by a stationary high density plasma spreading from the tip along the needle [18]. Owing to the rapid oscillation of the rf electric field, very few electrons are transported downstream of the active plasma region during operation [19], as a result, species

found downstream are transported mainly through diffusion and gas transport.

The kHz plasma jet and LTP are types of dielectric barrier discharge. The dielectric material prevents the discharges proceeding to arc formation. For the plasma jet, there is no ground electrode, therefore, higher voltages are required to break down the gas, and the plasma generated is often diffuse. The electric field in this configuration is parallel to the direction of gas flow. Electrons are transported axially by the electric field to a region downstream of the main discharge. This is critical for the creation of other charged and reactive species [19]. In the case of the LTP, a central ground electrode is present, this enhances the electric field along the tube axis and allows the plasma to be sustained at lower operating voltages [7]. In our case, a bright active plasma region is formed between the powered and ground electrode with a weaker afterglow region created downstream. Electrons and other energetic particles are created in this active region and are able to propagate downstream in a similar way to the plasma jet.

## Experimental

### Plasma Sources

**Plasma Needle** The rf plasma needle source used here was based on that described by Stoffels et al. [20], and was the same as that used in McKay et al. where a full description can be found [21]. The device was operated at 13.56 MHz in continuous rf and pulsed rf modes (duty cycles: 30%, 45%, 60%, and 90%). The average power applied to the needle was 3, 4.5, 6, and 9 W for the 30% to 90% duty cycles and 10 W for continuous wave excitation. The ceramic tube was fed with helium (purity: 99.996%) at a flow rate of 2 standard liters per min (SLM). The plasma was generated at the tip of the needle and was able to interact with the ambient air in the space between the ceramic tube exit, sample surface, and mass spectrometer extraction orifice. The size of the visible glow extending beyond the ceramic tube depended on whether the operation was pulsed or continuous but was ~1 mm in length. The plasma needle was fixed at a distance ~4 mm from the surface under analysis or the mass spectrometer extraction orifice. The plasma source was orientated at 45° to the sample surface. A diagram of the plasma needle and sample configuration is shown in Figure 1a.

**Plasma Jet** The plasma jet used in this study was a linear field dielectric barrier discharge (DBD), similar to that used by Walsh and Kong [19]. It consisted of a 12 cm glass capillary with a 2.4 mm inner diameter and 4.1 mm outer diameter. A copper ring electrode was attached 1 cm from the open end of the glass capillary and it was powered using a continuous wave kHz

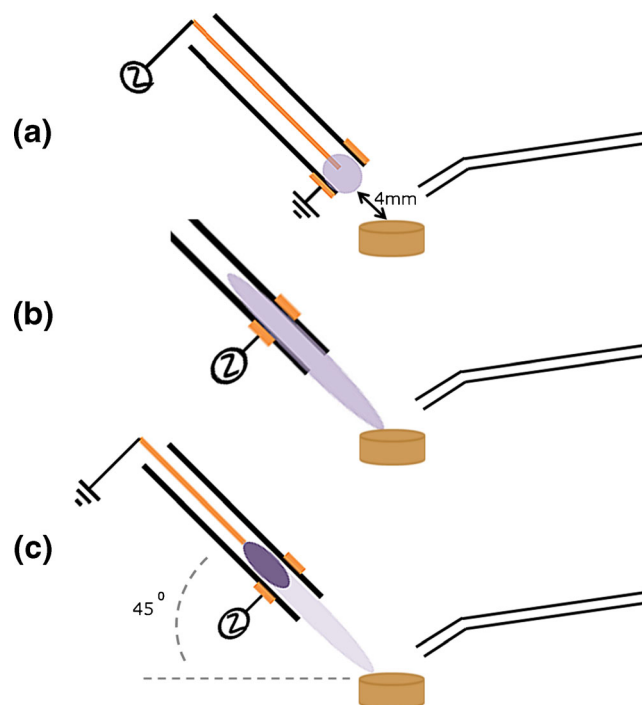


Figure 1. Plasma source, sample, and ‘sniffer’ tube configuration for (a) rf needle, (b) DBD jet, and (c) LTP

excitation source. The power supply consisted of a digital function generator (TG2000; AIM-TTI Instruments - Huntingdon, Cambridgeshire, UK) driving a commercial audio amplifier (HQ power, VPA2350MB) with a voltage step-up transformer (Express Transformers, Runcorn, UK) connected at the output stage, to generate the high voltages necessary for gas breakdown. The peak-to-peak voltage was fixed at 5.8 kV, and the frequency was varied from 5 to 20 kHz in 5 kHz increments. From current and voltage measurements, the average power applied to the plasma jet was found to increase from ~1.2 W to ~7.7 W as a function of increasing frequency. The tube was fed with pure He (99.996%) at a flow rate of 1.7 SLM. The helium was allowed to interact with the ambient air between the end of the tube and the sample/extraction orifice. The distance between the end of the tube and the sample was fixed at ~1 cm at an angle of 45°. The active plasma directly interacted with the sample/extraction orifice. A diagram of the plasma jet and sample configuration is shown in Figure 1b.

**LTP** The low temperature probes (LTP) construction was based on that used by Harper et al. [7]. It consisted of an adjustable grounded stainless steel central rod surrounded by a gas fed glass tube (inner diameter 4 mm). The central rod was positioned 3 cm from the end of the glass tube. A copper ring electrode was attached 1 cm from the end of the tube and was powered using a continuous wave kHz

excitation source. The power supply was the same as that used for the plasma jet. The peak-to-peak voltage was fixed to 5.8 kV, and the frequency was varied from 10 to 30 kHz in 10 kHz increments. From current and voltage measurements, the average power applied to the plasma jet was found to increase from ~2.3 W to ~6.4 W with increasing frequency. The tube was fed with pure He (99.996%) at a flow rate of 1.8 SLM and was allowed to interact with the ambient air between the end of the tube and the sample/extraction orifice. The distance between the sample and end of the tube was fixed at ~1 cm at an angle of 45°. The afterglow plasma directly interacted with the sample/extraction orifice. A diagram of the LTP and sample configuration is shown in Figure 1c.

### Instrumentation

To study the ions produced from each plasma source, a quadrupole-based mass spectrometer system, the HPR-60 molecular beam mass spectrometer (MBMS) from Hiden Analytical Ltd., Warrington, UK was utilized. The instrument has a mass range of 0–1000 Da with a resolution of 0.02 Da. This mass spectrometer was specifically designed for analysis of atmospheric pressure plasmas; a full description and diagram can be found in McKay et al. [21, 22]. The instrument was fitted with a 100  $\mu\text{m}$  grounded extraction orifice. By using a small extraction orifice, the chances of sampling a modified chemistry, which can be caused by electric field penetration into the low pressure regime, are reduced.

A Thermo Scientific Bremen, Germany LTQ Orbitrap Velos mass spectrometer was used to analyze the ions emitted from the samples using the plasma source. This instrument was used as it provides a high mass resolution of 100,000 at  $m/z$  400, making it ideal for analysis of complex surface chemistries. It was operated in both positive and negative ion mode. The mass spectrometer was programmed to collect up to a maximum Orbitrap injection time of 500 ms, using an automatic gain control (AGC) setting of  $5 \times 10^5$ . The AGC is designed to fill the trap with the optimal amount of ions to ensure that the signal intensities are high and that the spectra are not distorted by space-charging effects. The standard ion transfer tube was replaced with an extended version (127 mm), often referred to as the 'sniffer' tube. The 'sniffer' temperature was set to 275°C and was held at a voltage of 0 V. Samples were placed on a two-axis stage 1 mm below the sniffer.

### Analytes

The samples examined were a variety of common pharmaceutical products and polymers. This range of samples allowed us to test the viability and mass selectivity of each plasma ionization source. The pharmaceutical products used were paracetamol tablets (500 mg), ibuprofen gel (5% w/w), and caffeine (50 mg) tablets. These were all Superdrug Store plc. own brand products. The active ingredients in these

tablets have molecular masses of 151.1625, 206.2808, and 194.1905 Da, respectively. The tablets were placed onto glass slides whole and the ibuprofen gel was spread evenly in a thin layer across the slide. The polymers tested were polytetrafluoroethylene (PTFE) in the form of thread seal tape wrapped around a glass slide, poly(methyl methacrylate) (PMMA), and polylactic acid (PLA), which were deposited directly onto glass slides. These polymers consist of repeated structural units with unit molecular masses of 100.0149, 100.1157, and 72.0518 Da, respectively. The temperature that the samples reached during plasma exposure was recorded using a FLIR Systems, West Malling, Kent, UK InfraCAM thermal imager with an accuracy of  $\pm 2^\circ\text{C}$ . The FLIR Systems ThermoCAM Researcher Pro 2.9 software was used to process the thermal images. Variations in the emissivity of the different samples were not taken into account.

## Results

### Plasma Ion Chemistry

To determine the composition of each plasma source, the positive and negative ion mass spectra were acquired directly using the molecular beam mass spectrometer. The time-averaged spectra presented in Figures 2 and 3 were normalized to the total ion intensity in the mass range 0–100 Da, with the intensity expressed as a percentage. No significant peaks were detected outside of this mass range.

Figure 2a, b show the relative positive ion yield of the plasma needle operated in pulsed (45% duty cycle - 4.5 W) and continuous rf mode (10 W). The composition of the other duty cycles can be found in McKay et al. [21], which details the effect pulse modulating the rf needle has on the mass spectra composition. From Figure 2a, b and the results shown in McKay et al. [21], it can be seen that hydrated hydrogen ions  $[\text{H}^+(\text{H}_2\text{O})_n]$  dominate the positive ion spectrum, with larger clusters becoming increasingly dominant as the duty cycle was decreased. Figure 3a, b show the relative negative ion yield of the plasma needle in pulsed (45% duty cycle - 4.5 W) and continuous mode (10 W). For the pulse modulated cases hydrated air species  $\text{O}_2^-(\text{H}_2\text{O})_n$ ,  $\text{CO}_3^-(\text{H}_2\text{O})_n$ ,  $\text{HCO}_3^-(\text{H}_2\text{O})_n$ , etc., dominate the spectrum with the larger mass ions becoming increasingly dominant as the duty cycle was reduced [21]; however, for the continuous case, very few negative ions were detected.

Figures 2c, d and 3c, d show the relative positive and negative ion yield of the plasma jet operated at 10 and 20 kHz (~3.4 and ~7.7 W). It can be seen that the chemical composition was again heavily influenced by the interaction of the helium stream with the surrounding air, with the spectrum being dominated by oxygen and nitrogen species. The dominant positive ions were  $\text{N}^+$ ,  $\text{O}^+$ ,  $\text{N}_2^+$ , and  $\text{O}_2^+$ , and the dominant negative ions were  $\text{O}^-$ ,  $\text{O}_2^-$ ,  $\text{NO}_2^-$ , and  $\text{NO}_3^-$ . As the frequency of the discharge was increased the yield of the positive and negative ions detected did not change significantly, however, the ratio of negative to positive ion

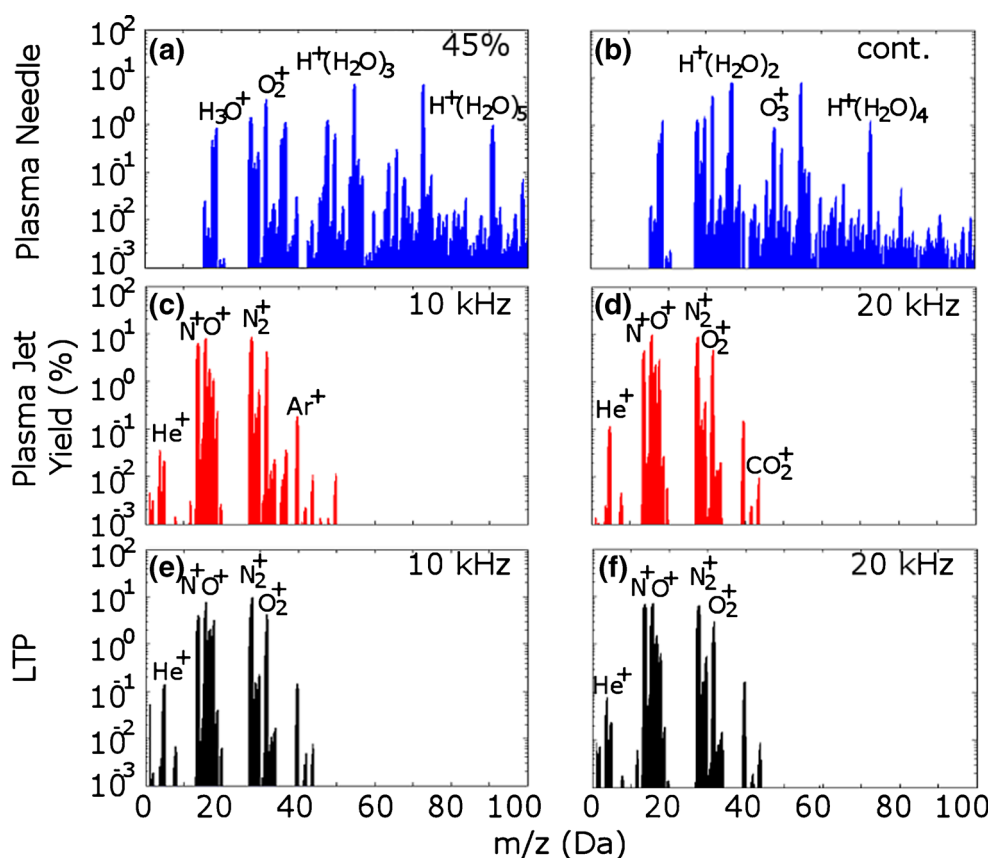


**Figure 2.** Positive ion mass spectra acquired on the Hiden MBMS for (a) pulsed rf – duty cycle, 45%, power, 4.5 W, (b) continuous rf – power, 10 W, (c) plasma jet – frequency, 10 kHz, power, 3.4 W, (d) plasma jet – frequency, 20 kHz, power, 7.7 W, (e) LTP – frequency, 10 kHz, power, 2.3 W, and (f) LTP – frequency, 20 kHz, power, 4.6 W

intensities (not shown here) decreased, suggesting that the discharge became more electropositive at higher frequencies. In electropositive plasmas, the negative charge is carried predominantly by the electrons, and this may have an effect on the ability of the plasma to desorb/ionize material from the surface.

In Figures 2e, f and 3e, f the relative positive and negative ion yields of the LTP, for 10 and 20 kHz ( $\sim 2.3$  and  $\sim 4.6$  W) are shown. From these figures, it can be seen that the ions present were similar to those produced in the plasma jet. It should again be noted that although the ion composition of the LTP did not change significantly as frequency increased, the ratio of negative-to-positive ion intensities decreased.

### Surface Analysis

To assess the effectiveness of these three plasma sources to desorb and ionize surface compounds, the Orbitrap MS was used in both positive and negative ion mode in  $m/z$  range 50–1500 Da. The background spectrum, obtained when there was only a blank glass slide present, was removed from the sample spectra. To allow comparison between the

three sources, the ion intensities have been plotted against average power.

Figure 4a–c show the time-averaged intensities (c/s) of the main negative ions obtained from analysis of ibuprofen gel. In the case of the pulse-modulated plasma needle, the main negative ions detected had masses of 205.123 and 221.118 Da. These correspond to a deprotonated ibuprofen ( $[M - H]^-$ ) and oxygenated ibuprofen ( $[M - H + O]^-$ ). As the average power applied to the plasma needle increased the intensity of  $[M - H]^-$  increased. The intensity of  $[M - H + O]^-$  was also seen to increase as the average power increased from 3 to 9 W. In continuous mode (10 W) a small decrease in intensity was observed. For the plasma jet the main negative ions detected had masses of 75.045, 151.097, and 205.123 Da, corresponding to deprotonated propylene glycol ( $[C_3H_8O_2 - H]^-$ ), clustered propylene glycol ( $[2(C_3H_8O_2) - H]^-$ ) and deprotonated ibuprofen ( $[M - H]^-$ ). As the average power of the plasma jet increased from  $\sim 1.1$  to  $\sim 7.7$  W (5–20 kHz), the general trend of the ions was one of increasing intensity. For the LTP (Figure 4c), only three different frequencies were studied and, as a result, a trend cannot be directly inferred for these results. It was observed that the main ions detected were the same as for the plasma jet. It was again observed that as the average power within

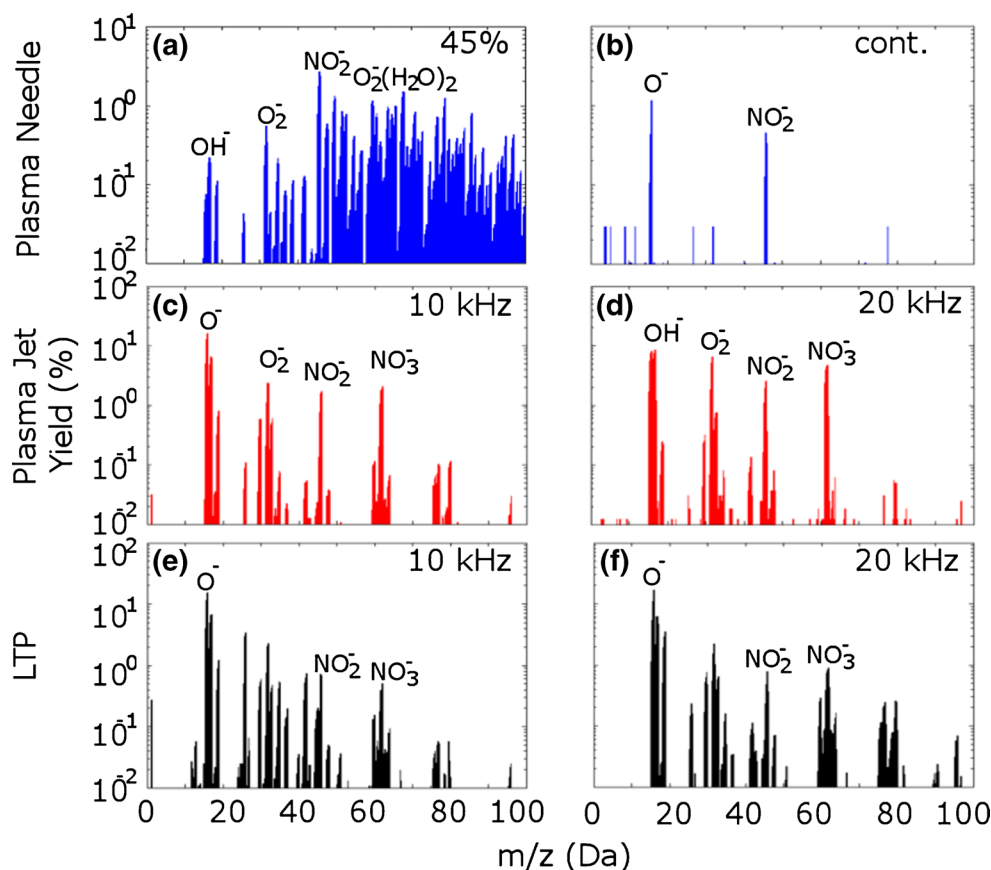


**Figure 3.** Negative ion mass spectra acquired on the Hiden MBMS for (a) Pulsed rf – duty cycle, 45%, power, 4.5 W, (b) Continuous rf – power, 10 W, (c) plasma jet – frequency, 10 kHz, power, 3.4 W, (d) plasma jet – frequency, 20 kHz, power, 7.7 W, (e) LTP – frequency, 10 kHz, power, 2.3 W, and (f) LTP – frequency, 20 kHz, power, 4.6 W

the discharge increased from  $\sim 2.3$  to  $\sim 6.4$  W (10–30 kHz) the intensity of the deprotonated ibuprofen ion increased. Propylene glycol and its cluster ion also displayed an initial increase in intensity. At higher powers, a sharp decrease in intensity was observed. From Figure 4, it is also observed that the ion intensities detected by the three plasma sources varies significantly. The ion intensities when analyzing with the LTP are approximately a factor of 10 lower than the plasma needle, and those from the plasma jet are a factor of 100 lower.

Paracetamol was only detected when using the plasma needle, Figure 5 shows the time-averaged intensities (c/s) of the main positive ions detected. The main ions were detected at masses of 110.061, 152.071, and 303.135 Da, corresponding to the protonated paracetamol ion with the loss of a ketone ( $[M+H_2-C_2H_3O]^+$ ), the protonated paracetamol ion ( $[M+H]^+$ ) and the protonated dimer paracetamol ion ( $[2M+H]^+$ ). From Figure 5 it can be seen that these ions were not detected until the duty cycle was greater than 45% (4.5 W); above 90% (9 W) the ion intensity decreased.

Figure 6a–c show the time-averaged intensities for the dominant positive ions detected for caffeine tablets. The main ions detected for all three sources were at masses 142.062 and 195.089 Da. These correspond to a fragment of

the caffeine molecule ( $[C_5H_8O_2N_3]^+$ ), and the protonated caffeine ion ( $[M+H]^+$ ). In general the intensity of the main molecular ion increased as average power was increased for all of the sources. Again, as was seen for ibuprofen, the signal intensities vary greatly between the three plasma sources, with those for the plasma needle being many orders of magnitude greater than the LTP and plasma jet. However, here the ion intensities from the plasma jet are similar to those from the LTP.

Mass spectra from polymers are generally characterized by a series of mass peaks made from a number of linked base units [15]. Figure 7a–c show the PTFE peaks obtained for the pulse-modulated rf plasma needle (duty cycle 60%, 6 W), the plasma jet (20 kHz,  $\sim 7.7$  W) and the LTP (20 kHz,  $\sim 4.6$  W). From Figure 7, it can be seen that the plasma needle was able to detect PTFE in a significantly higher mass range than the plasma jet and LTP. For the plasma needle the largest series detected was  $[(CF_2)_n+C_2O_4H]^-$  in the mass range 300–1000 Da; below this range PTFE peaks were not detected. For the plasma jet (Figure 7b) and the LTP (Figure 7c) increased fragmentation was observed compared with the plasma needle, with several different series appearing in the mass range 100–800 Da. For the plasma jet and LTP, three main series' observed were

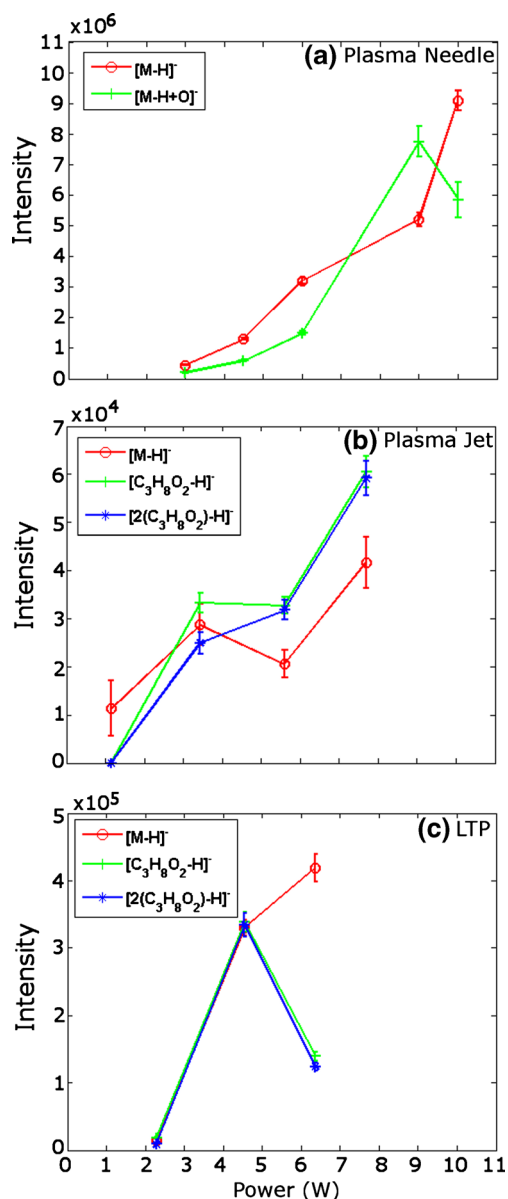


**Figure 4.** Dominant negative ion intensities for ibuprofen gel acquired on the Orbitrap MS, (a) rf plasma needle – duty cycle, 30%–100%, power, 3–10 W, (b) plasma jet – frequency, 5–20 kHz, power, 1.1–7.7 W, and (c) LTP – frequency, 10–30 kHz, power, 2.3–6.4 W

$[C_2F+(CF_2)_n+O_3]^-$ ,  $[CF+(CF_2)_n+O_2]^-$ , and  $[CF+(CF_2)_n+O]^-$ .

Figure 8a–c shows peaks obtained for PMMA, obtained for the pulse modulated rf plasma needle (duty cycle 60%, 6 W), the plasma jet (20 kHz, ~7.7 W), and the LTP (20 kHz, ~4.6 W). PMMA can be detected in both positive and negative ion mode but for the majority of cases considered here the spectrum was clearest in the negative ion mode, with the exception of the continuous rf needle where the positive ion spectra was clearest (not shown here). Unlike the PTFE spectra the mass range of the detected PMMA ions for the three plasma sources is the same. For the

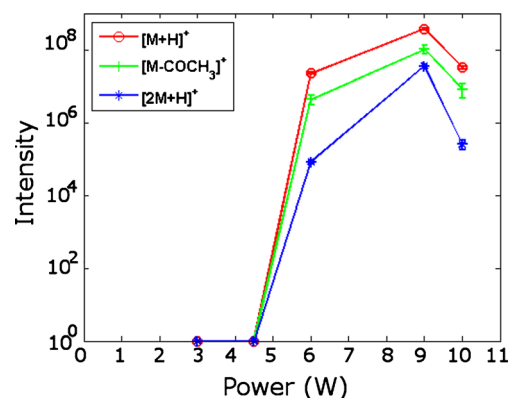


**Figure 5.** Dominant positive ion intensities for paracetamol acquired on the Orbitrap MS using the rf plasma needle – duty cycle, 30%–100%, power, 3–10 W

pulse modulated plasma needle the three main polymer series identified were,  $[M_n-C_2H_5+O_x]^-$ ,  $[M_n-CH_3+O_x]^-$ , and  $[M_n-CH_2+O_x]^-$  in the mass range 250–450 Da. For the plasma jet and LTP, several different series were present; the four main series identified were  $[M_n-H_5+O_x]^-$ ,  $[M_n-CH_7+O_x]^-$ ,  $[M_n-CH_5+O_x]^-$ , and  $[M_n-H_7+O_x]^-$  in the 250–450 Da mass range. For PLA the peaks detected observed a similar trend to that seen for PMMA and are, therefore, not shown here.

## Discussion

### Plasma Ion Chemistry

The background ion species detected for all of the sources result from the interaction of the helium plasma with the surrounding air. Small positive ion species were most likely formed through direct electron impact ionization, Penning, and step ionization with the helium metastables and dimer metastables present within the discharge. Helium metastables have much higher energies ( $\epsilon \sim 19.8$  and  $18.4$  eV) than that required for ionization of air species, for example the ionization energy of nitrogen and oxygen is 15.6 and 12.1 eV, respectively [23, 24]. For the plasma needle the ionized water clusters were formed through hydration of these smaller ionized molecules, where the rate of hydration reactions is inversely proportional to gas temperature [25]. The shift in yield from low mass water clusters to high mass water clusters as the duty cycle was reduced suggests that the gas temperature was decreasing. This was confirmed in a previous contribution by thermal imaging of the plasma needle tip, where the temperature was seen to decrease from 99.1 to 44.1°C as the duty cycle was reduced from 90% to 30% [21]. Such gas temperatures are similar to those calculated by Stoffels et al. [26, 27], from measurements of helium density fraction as a function of power and optical emission spectroscopy. For the plasma jet and LTP, the water cluster ions were not present. This is thought to be due to these sources having direct contact with the extraction orifice/surface and a higher gas velocity (gas velocity [m/s] = gas flow rate

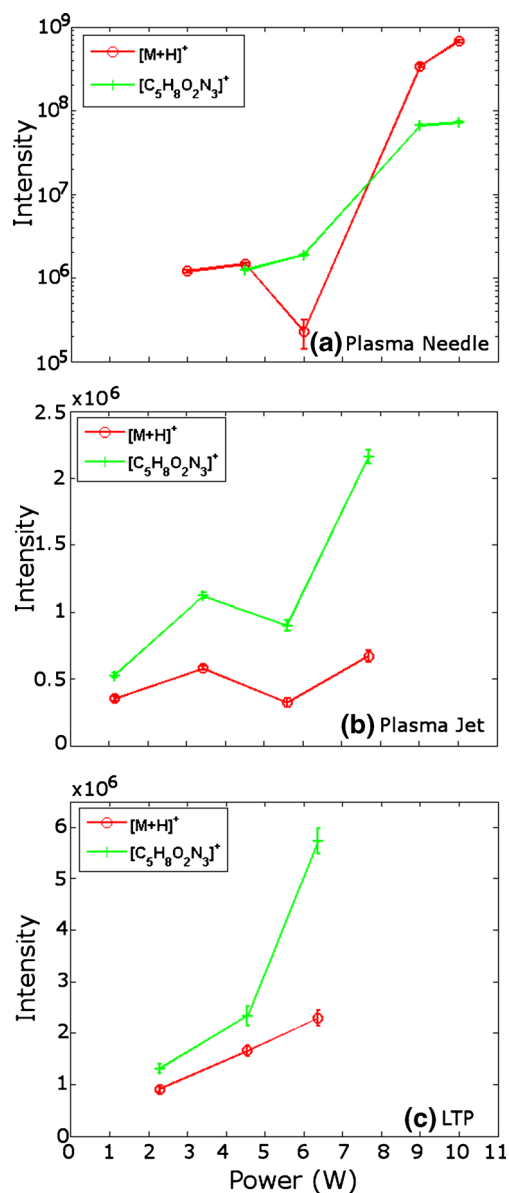


**Figure 6.** Dominant positive ion intensities for caffeine tablets acquired on the Orbitrap MS: (a) rf plasma needle – duty cycle, 30%–100%, power, 3–10 W, (b) plasma jet – frequency, 5–20 kHz, power, 1.1–7.7 W, and (c) LTP – frequency, 10–30 kHz, power, 2.3–6.4 W

$[m^3/s]/\text{area of tube } [m^2]$ , resulting in a higher helium fraction at the extraction orifice and less time available for the formation of larger ions. The amount of water entrained into the plasma plume may influence desorption/ionization processes at the sample surface. From thermal imaging, the gas temperature at the exit of the jet was  $\sim 25$  to  $\sim 28^\circ\text{C}$ , for operating frequencies of 5–20 kHz. For the LTP the gas temperature approximated from thermal imaging was between  $\sim 30$  to  $\sim 43^\circ\text{C}$ , for operating frequencies of 10–30 kHz.

Small negative ions were most likely formed through dissociative electron attachment reactions and attachment

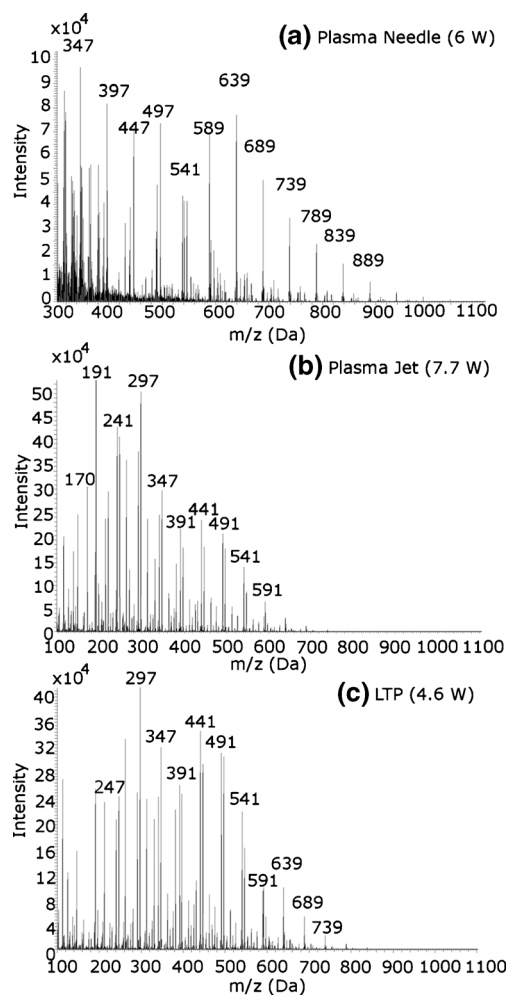


**Figure 7.** Negative ion spectra of PTFE acquired on the Orbitrap MS for (a) rf plasma needle – duty cycle, 60%, power, 6 W, (b) plasma jet – frequency, 20 kHz, power, 7.7 W, and (c) LTP – frequency, 20 kHz, power, 4.6 W

reactions with the molecules in air, with larger ions again formed through hydration. From time-resolved measurements presented in McKay et al. it was found that for the plasma needle the negative ions were mainly produced during the off-phase of the discharge [21]. The increased formation during the off-phase is due to the release of electrons from the active plasma region when the external electric field is no longer present. This was coupled with a reduction in the gas temperature, allowing increased negative water cluster formation. In the continuous case considered here, negative ion production was inhibited by the high gas temperature and the highly transient electric field, which confine the electrons that are essential for negative ion formation in the afterglow. This results in very few negative ions being detected in this mode.

### Surface Analysis

To explain the trend of the ion intensities obtained from surface analysis, the electric field, the propagation mecha-

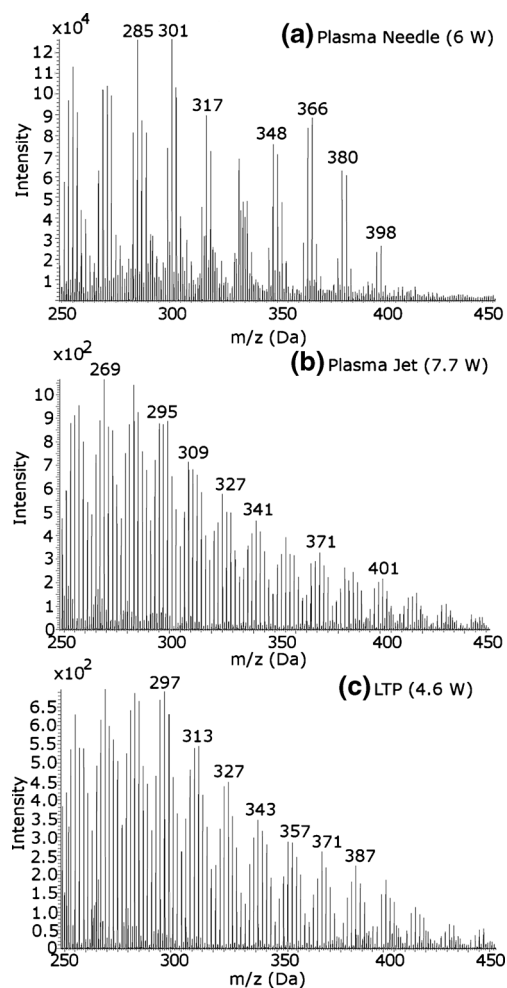


**Figure 8.** Negative ion spectra of PMMA acquired on the Orbitrap MS for (a) rf plasma needle – duty cycle, 60%, power, 6 W, (b) Plasma Jet – frequency, 20 kHz, power, 7.7 W, and (c) LTP – frequency, 20 kHz, power, 4.6 W

nisms of the plasma species and the surface temperature of the samples must be taken into account.

The main species transport mechanisms for the rf plasma needle were diffusion and gas transport. This is due to the highly transient nature and orientation of the electric field, which act to confine the plasma to a small region around the plasma needle tip [19]. As a result of this confinement, the sample was not exposed directly to the active plasma region or the strong electric fields. From thermal imaging it was found that the average surface temperature of the samples ~4 mm downstream for the continuous rf case and the pulse modulated cases (duty cycle 90%–30%) were ~87, 63, 43, 36, and 29°C, respectively. For the plasma needle, the general trend of the molecular ion ( $[M\pm H]^\pm$ ) for ibuprofen, paracetamol, and caffeine was one of increasing intensity as the duty cycle and average power increased. This increase is correlated with the increase in surface temperature of the samples. This suggests that thermal processes are more

important for desorption/ionization in this source than the ion content of the plasma or electric field interaction. These results are consistent with previous studies, which have shown that increases in surface temperature promote thermal emission of material from samples [15].

For the dielectric barrier plasma jet, the species transport mechanisms are very different from that of the plasma needle, and they have been widely documented [28–32]. Owing to the direct contact between the plasma plume and surface, the surface is exposed to the strong self-induced electric fields and energetic particles that are associated with the streamer formed in this type of discharge. This bombardment of the surface by high electric field and energetic particles may be significant in the desorption/ionization process [33]. The average surface temperature of the samples was ~29, 30, 31, and 31°C for the 5, 10, 15, and 20 kHz plasma jet, respectively. In general, the trends of the ibuprofen and caffeine molecular ions showed an increase in intensity as the frequency and average power increased as the temperature of the samples remained relatively constant; this is thought to be predominantly linked to the increased surface bombardment experienced by the sample from the streamers.

Unlike the plasma jet and rf needle, the transport properties of the LTP are not well documented. To allow us to better understand the propagation mechanisms of this plasma source, a high speed ICCD camera was used to image the helium emission from the discharge over the 20 kHz cycle (not shown here). From the ICCD images, voltage, and current waveforms, it was found that the propagation mechanisms of the reactive species are similar to those described for the plasma jet. This suggests that surface bombardment by these ionization fronts may again have an important role in desorption/ionization. For the LTP, thermal processes on the surface may also be of importance. The average sample surface temperatures for 10, 20, and 30 kHz were ~31, 35 and 40°C. This is a greater increase than that shown by the plasma jet and clearly shows a dependence on frequency. This increase in heating may be linked to the enhanced electric field that is created because of the central grounded rod [19]. These results suggest that thermal processes, surface bombardment, and electric field may be important for the LTP, this was further confirmed by the increase in intensity seen for the molecular ions of caffeine and ibuprofen.

The variation in temperatures between the plasma sources could also explain the difference in ion intensities that are recorded for the analysis of the pharmaceuticals. From Salter et al. it is shown that for pharmaceuticals, their vapor pressure is a function of surface temperature [34]. For example, paracetamol has vapor pressures ranging between 0.0671 and 0.000022 Pa for the temperature range 74–40°C, and ibuprofen had a vapor pressure ranging from 3.386 to 0.00708 Pa for the temperature range 70.4–25 °C [34]. As a result of this relationship, the only source that can desorb/ionize surface material from paracetamol is the plasma



needle when it achieves a surface temperature greater than 40°C. It also explains why plasma needle and LTP achieved higher signal intensities than the plasma jet.

For the polymers, it is again seen that surface temperature and species propagation mechanisms heavily influence the mass spectra obtained for each source. For the plasma jet and LTP, the bombardment of the surface by the energetic particles and the strong electric fields resulted in increased fragmentation of the polymer chains. For the plasma needle, in the case of PTFE, the higher surface temperatures result in increased thermal emission allowing larger polymer chains to be released from the surface. The indirect treatment method of the plasma needle also reduced fragmentation for both PTFE and PMMA, resulting in a simpler mass spectrum with a greater sensitivity in the higher mass range.

## Conclusions

In this study, we have compared three low-temperature atmospheric pressure plasma sources used in ambient surface analysis mass spectrometry. It was found that the ion chemistry for each source was heavily influenced by air species due to gas mixing and helium metastable Penning ionization reactions. In general, all sources were able to ionize the majority of samples. The plasma needle had the advantage of being able to desorb/ionize surface compounds without direct contact, and it also effectively induced thermal emission from surfaces at higher average powers. This was beneficial when the sample was compact, well adhered to the surface, or had a high vapor pressure, but care must be taken when treating heat sensitive material. The plasma jet kept an almost constant sample surface temperature for all frequencies, this is an advantage when treating heat sensitive material such as biological tissue. Owing to the streamer-like nature of the jet, strong electric fields and energetic particles directly interacted with the surface. It was found that increasing the frequency allowed more surface material to be removed from the surface. The LTP was found to have similar species propagation mechanisms to that of the plasma jet and was also able to remove more surface material with increased frequency. The LTP was also able to induce thermal emission at higher frequencies because of the enhanced electric field, which may in the future allow increased control over the surface treatment conditions.

## Acknowledgments

The authors thank the University of Liverpool for providing support for this project. This work is also partially supported by the Chemical and Biological Program of the National

Measurement System of the UK Department of Business, Innovation, and Skills.

## References

- Williams, J.P., Scrivens, J.H.: Rapid accurate mass desorption electrospray ionization tandem mass spectrometry of pharmaceutical samples. *Rapid Commun. Mass Spectrom.* **19**, 3643–3650 (2005)
- Ratcliffe, L.V., Rutten, F.J.M., Barrett, D.A., Whitmore, T., Seymour, D., Greenwood, C., Aranda-Gonzalvo, Y., Robinson, S., McCoustra, M.: Surface analysis under ambient conditions using plasma-assisted desorption/ionization mass spectrometry. *Anal. Chem.* **79**, 6094–6101 (2007)
- Symonds, J.M., Galhena, A.S., Fernandez, F.M., Orlando, T.M.: Microplasma discharge ionization source for ambient mass spectrometry. *Anal. Chem.* **82**, 621–627 (2010)
- Marotta, E., Paradisi, C.: A mass spectrometry study of alkanes in air plasma at atmospheric pressure. *J. Am. Soc. Mass Spectrom.* **20**, 697–707 (2009)
- Green, F.M., Salter, T.L., Stokes, P., Gilmore, I.S., Connor, G.O.: Ambient mass spectrometry: advances and applications in forensics. *Surf. Interface Anal.* **42**, 347–357 (2010)
- Benassi, M., Berisha, A., Romao, W., Babayev, E., Rompp, A., Spengler, B.: Petroleum crude oil analysis using low-temperature plasma mass spectrometry. *Rapid Commun. Mass Spectrom.* **27**, 825–834 (2013)
- Harper, J.D., Charipar, N.A., Mulligan, C.C., Zhang, X., Cooks, R.G., Ouyang, Z.: Low-temperature plasma probe for ambient desorption ionization. *Anal. Chem.* **80**, 9097–9104 (2008)
- Xing, Z., Wang, J., Han, G., Kuermaiti, B., Zhang, S., Zhang, X.: Depth profiling of nanometer coatings by low temperature plasma probe combined with inductively coupled plasma mass spectrometry. *Anal. Chem.* **82**, 5872–5877 (2010)
- Cody, R.B., Laramée, J.A., Durst, H.D.: Versatile new ion source for the analysis of materials in open air under ambient conditions. *Anal. Chem.* **77**, 2297–2302 (2005)
- Shelley, J.T., Wiley, J.S., Chan, G.C.Y., Schilling, G.D., Ray, S.J., Hieftje, G.M.: Characterization of direct-current atmospheric-pressure discharges useful for ambient desorption/ionization mass spectrometry. *J. Am. Soc. Mass Spectrom.* **20**, 837–844 (2009)
- Pfeuffer, K.P., Shelley, J.T., Ray, S.J., Hieftje, G.M.: Visualization of mass transport and heat transfer in the FAPA ambient ionization source. *J. Anal. At. Spectrom.* **28**, 379–387 (2013)
- Na, N., Zhao, M., Zhang, S., Yang, C., Zhang, X.: Development of a dielectric barrier discharge ion source for ambient mass spectrometry. *J. Am. Soc. Mass Spectrom.* **18**, 1859–1862 (2007)
- Hayen, H., Michels, A., Franzke, J.: Dielectric barrier discharge ionization for liquid chromatography/mass spectrometry. *Anal. Chem.* **81**, 10239–10245 (2009)
- Bowfield, A., Barrett, D.A., Alexander, M.R., Ortori, C.A., Rutten, F.M., Salter, T.L., Gilmore, I.S., Bradley, J.W.: Surface analysis using a new plasma assisted desorption/ionization source for mass spectrometry in ambient air. *Rev. Sci. Instrum.* **83**, 063503, 1–7 (2012)
- Salter, T.L., Gilmore, I.S., Bowfield, A., Olabanji, O.T., Bradley, J.W.: Ambient surface mass spectrometry using plasma-assisted desorption ionization: effects and optimization of analytical parameters for signal intensities of molecules and polymers. *Anal. Chem.* **85**, 1675–1682 (2013)
- Kruger, C.H., Owano, T.G., Laux, C.O.: Experimental investigation of atmospheric pressure nonequilibrium plasma chemistry. *IEEE Trans. Plasma Sci.* **25**, 5, 1042–1051 (1997)
- Schutze, A., Jeong, J.Y., Babayan, S.E., Park, J., Selwyn, G.S., Hicks, R.F.: The atmospheric-pressure plasma jet: a review and comparison to other plasma sources. *IEEE Trans. Plasma Sci.* **26**, 6, 1685–1694 (1998)
- Sakiyama, Y., Graves, D.B.: Corona-glow transition in the atmospheric pressure rf-excited plasma needle. *J. Phys. D: Appl. Phys.* **39**, 3644–3652 (2006)
- Walsh, J.L., Kong, M.G.: Contrasting characteristics of linear-field and cross-field atmospheric plasma jets. *Appl. Phys. Lett.* **93**, 111501, 1–3 (2008)
- Stoffels, E., Kieft, I.E., Sladek, R.E.J., van den Bedem, L.J.M., van der Laan, E.P., Steinbuch, M.: Plasma needle for in vivo medical treatment: recent developments and perspectives. *Plasma Sources Sci. Technol.* **15**, S169–S180 (2006)

21. McKay, K., Walsh, J.L., Bradley, J.W.: Observations of ionic species produced in an atmospheric pressure pulse-modulated rf plasma needle. *Plasma Sources Sci. Technol.* **22**, 035005, 1–8 (2013)
22. McKay, K., Oh, J.-S., Walsh, J.L., Bradley, J.W.: Mass spectrometric diagnosis of an atmospheric pressure helium microplasma jet. *J. Phys. D. Appl. Phys.* **46**, 464018, 1–9 (2013)
23. Kramida A., Ralchenko Y., Reader J., NIST ASD Team 2012 NIST Atomic Spectra Database: (ver. 5.0) (Gaithersburg, MD: National Institute of Standards and Technology). Available at: <http://physics.nist.gov/asd>. Accessed September 12 (2013)
24. Lias, S.G.: NIST Webbook (Gaithersburg, MD: National Institute of Standards and Technology). Available at: <http://webbook.nist.gov/chemistry/> Accessed September 23 (2013)
25. Liu, D.X., Bruggeman, P., Iza, F., Rong, M.Z., Kong, M.G.: Global model of low-temperature atmospheric-pressure He+H<sub>2</sub>O plasmas. *Plasma Sources Sci. Technol.* **19**, 025018, 1–22 (2010)
26. Stoffels, E., Flikweert, A.J., Stoffels, W.W., Kroesen, G.M.W.: Plasma needle: a non-destructive atmospheric plasma source for fine surface treatment of (bio) materials. *Plasma Sources Sci. Technol.* **11**, 383–388 (2002)
27. Stoffels, E., Aranda-Gonzalvo, Y., Whitmore, T.D., Seymour, D.L., Rees, J.A.: A plasma needle generates nitric oxide. *Plasma Sources Sci. Technol.* **15**, 501–506 (2006)
28. Karakas, E., Koklu, M., Larroussi, M.: Correlation between helium mole fraction and plasma bullet propagation in low temperature plasma jets. *J. Phys. D. Appl. Phys.* **43**, 155202, 1–5 (2010)
29. Breden, D., Miki, K., Raja, L.L.: Computational study of cold atmospheric nanosecond pulsed helium plasma jet in air. *Plasma Sources Sci. Technol.* **21**, 034011, 1–13 (2012)
30. Lu, X., Laroussi, M., Puech, V.: On atmospheric-pressure non-equilibrium plasma jets and plasma bullets. *Plasma Sources Sci. Technol.* **21**, 034005, 1–17 (2012)
31. Raizer, Y.P.: *Gas Discharge Physics*. Springer, Berlin, 334–338 (1991)
32. Algwari, Q.T., O’Connell, D.: Electron dynamics and plasma jet formation in a helium atmospheric pressure dielectric barrier discharge jet. *Appl. Phys. Lett.* **99**, 121501, 1–2 (2011)
33. Babaeva, N.Y., Kushner, M.J.: Control of ion activation energy delivered to tissue and sensitive materials in atmospheric pressure plasmas using thin porous dielectric sheets. *J. Phys. D. Appl. Phys.* **46**, 125201, 1–9 (2013)
34. Salter, T. L., Bunch, J., Gilmore, I.S.: The importance of sample form and surface temperature for analysis by ambient plasma mass spectrometry (PADI). *Anal. Chem.* Submitted 27 March (2014)